ACS APPLIED MATERIALS & INTERFACES

RESEARCH ARTICLE

www.acsami.org

Polyoxometalate-Assisted Synthesis of TiO_2 Nanoparticles and Their Applications in Aqueous Hybrid Electrochemical Capacitors

Jiao Yin,[†,‡] Li Qi,[†] and Hongyu Wang*[,†]

[†]State Key Laboratory of Electroanalytical Chemistry, Changchun Institute of Applied Chemistry, Chinese Academy of Sciences, 5625 Renmin Street, Changchun 130022, China

[‡]Graduate School of Chinese Academy of Sciences, Beijing 100039, China

Supporting Information

ABSTRACT: A mild hydrolysis method was proposed to synthesize TiO_2 nanoparticles (NPs), in which polyoxometalate adjusted the hydrolyzation reaction rate and controlled the size of TiO_2. The resultant TiO_2 NPs were fully characterized via XRD, SEM, TEM, XPS. The electrochemical investigations demonstrated that the as-obtained TiO_2 NPs delivered higher specific capacitance than that of bulk and commercial samples in lithium-ion aqueous solution. Furthermore, the charge storage mechanism of TiO_2 NPs was also studied. More importantly, the aqueous hybrid capacitors based on activated carbon (AC) and TiO_2 were constructed and their electrochemical performance were fully investigated in aqueous solutions.

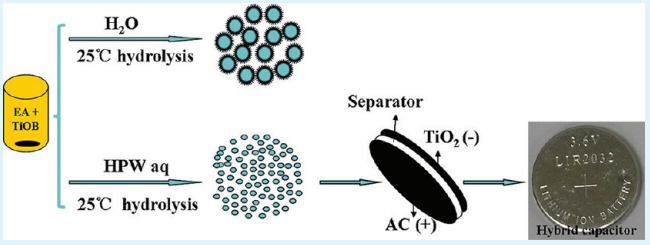

KEYWORDS: polyoxometalate, TiO_2, nanoparticles, hybrid, electrochemical capacitors

1. INTRODUCTION

Nowadays, electrochemical capacitors have been considered as promising electric energy storage devices in the world.[1−4] During the past decade, some significant improvements have been made in elevating energy density levels of electrochemical capacitors. One representative is the invention of hybrid capacitors based on a porous carbon electrode and a battery-type electrode.[5−7] As compared with the traditional electric double-layer capacitors (EDLCs) which are composed of two symmetrical porous carbon electrodes, hybrid capacitors usually have higher working voltage and specific capacitance values. In such cases, the choice of the battery-type electrode is a key point in constructing a satisfactory hybrid capacitor. Although most of the disciplines in designing battery electrode materials still hold here, there should be some modifications of these standards to cater to the practical needs of electrochemical capacitors.[8,9]

TiO_2 has been proved as an advantageous electrode material in lithium-ion batteries because of a series of merits like safety, abundance on the earth, low cost, and environmental benignity.[10−12] Recently, titanate-based negative electrode materials have also been applied in lithium-ion capacitors. In these energy storage devices, the Li^+-based non-aqueous electrolyte solutions are usually utilized in conjunction with nanostructured TiO_2 electrode material.[13−15] More recently, it was found that lithium insertion into meso-porous TiO_2 from aqueous solution is feasible, and the electrochemical capacitor composed of "all-nanostructured" Li_xTiO_2 and $NiOOH_{2-x}$ was proposed.[16] From the viewpoint of practical applications, aqueous solutions possess considerable merits. For example, high ion conductivity of aqueous electrolyte offsets the low electronic conductivity of TiO_2.

However, electrochemical capacitor, as a practical device, the configuration should be simplified. The complex configuration of the "all-nanostructured" Li_xTiO_2 and $NiOOH_{2-x}$ capacitor is unfavorable for evaluation of each single elecstrode because it is difficult to gain capacity contributions of each single electrode to full cell. Furthermore, we found it hard to investigate the electrochemical property of single electrode when two electrodes synchronously occur faradaic reactions. In such cases, positive electrode can be replaced by activated carbon (AC). Simple aqueous hybrid capacitor containing porous carbon electrode and nanostructured TiO_2 electrode could be proposed so as to better study the charge storage mechanism of TiO_2 single electrode as well as the electrochemical performance of hybrid capacitor (AC/TiO_2). In addition, for practical applications, the reversibility and cycling life of the full cell should be investigated in detail. Thus, it became an urgent task to study the electrochemical performance of full cell (AC/TiO_2), and to discover the charge storage behavior of the TiO_2 single electrode in aqueous solution.

Nano-sized materials brought several merits like more active sites, short diffusion path lengths, and easy access to electrolyte. Herein, we will introduce a mild hydrolysis method to synthesize TiO_2 nanoparticles (NPs). In this route, different concentrations of polyoxometalate were utilized to adjust the hydrolyzation reaction rate and control the size of TiO_2. Concentrated polyoxometalate resulted in smaller-sized TiO_2 NPs. Then the charge storage behavior of the as-obtained TiO_2 NPs was studied in

Received: July 27, 2011
Accepted: October 11, 2011
Published: October 11, 2011

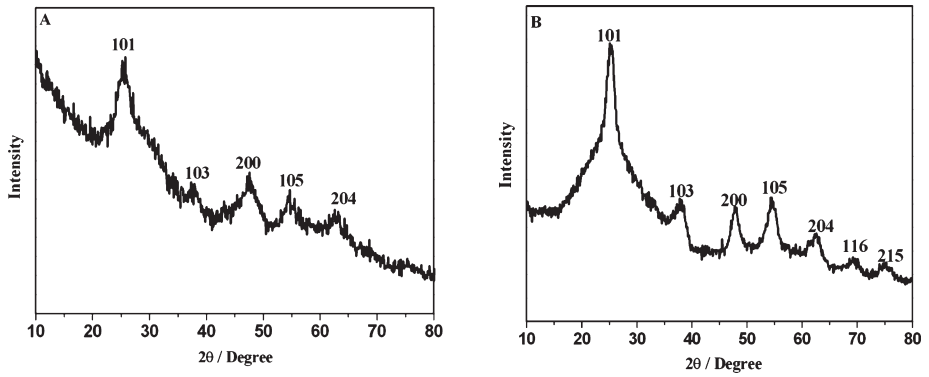

Figure 1. XRD patterns of (A) T-02 and (B) T-02c.

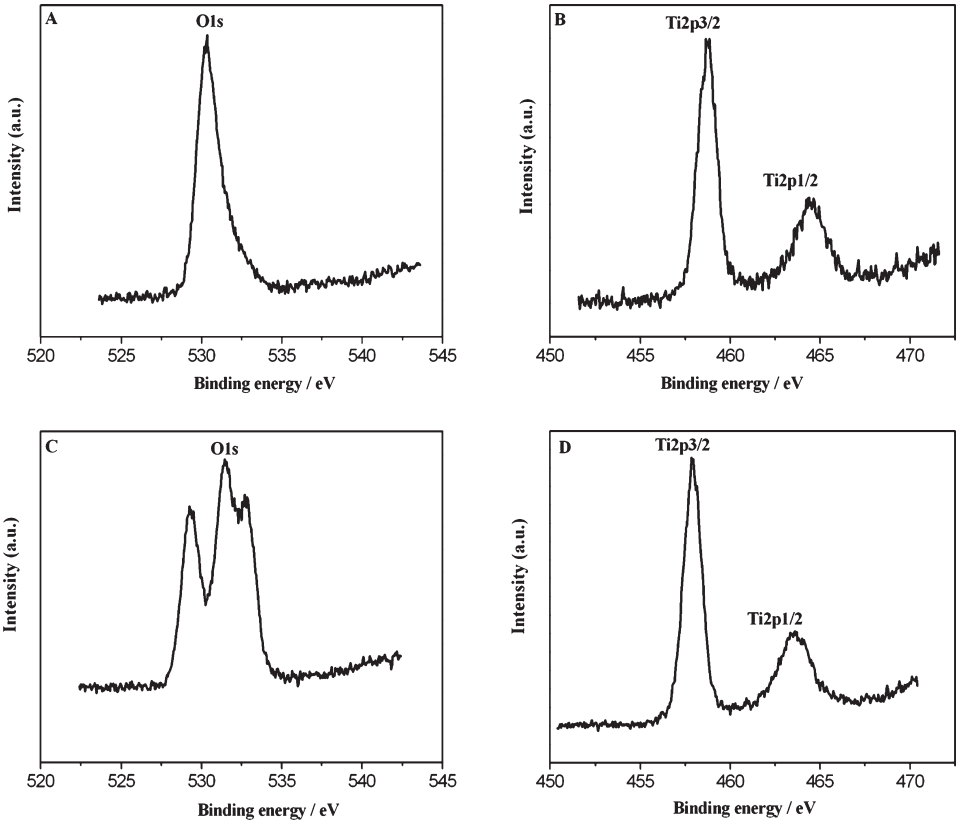

Figure 2. O1s XPS spectra of (A) T-02 and (C) T-0. Ti2p XPS spectra of (B) T-02 and (D) T-0.

neutral aqueous solutions (Li^+, Na^+, K^+). Finally, a series of hybrid aqueous capacitors based on activated carbon and TiO_2 (AC/TiO_2) were constructed.

2. EXPERIMENTAL SECTION

2.1. Chemicals and Reagents. Tetrabutyl titanate (TBT) and Polyoxometalate (12-tungstophosphoric acid, $H_3PW_{12}O_{40}.nH_2O$, HPW) were obtained from Fluka. P25 (commercial TiO_2 powder, which consists of about 25% rutile and 75% anatase and has a particle size of about 30 nm) was purchased from Aldrich. Ethyl acetate was purchased from Beijing Fine Chemical Company. Other chemicals and reagents were of analytical grade, and all the reagents were used as received without further purification.

2.2. Preparation of TiO_2. In a typical experiment, a mixed solution containing 2 mL TBT and 6 mL ethyl acetate was magnetically stirred at room temperature. After 0.5 h, 3 mL HPW solution was dropwise added under vigorously stirring. HPW solid was dissolved in deionised water to form a final concentration of 0.1, 0.2, and 0.4 mol L^{-1}, respectively. The resulting suspension was stirred for another 3 h, followed by collection. The obtained solid product was exhaustively washed with ethanol and deionised water, dried at 60 °C. To improve the crystallinity of the products, we calcined the samples at 500 °C in air. These samples are listed in Table S1 (see the Supporting Information).

2.3. Characterization Methods. X-ray diffraction (XRD) patterns of the samples were recorded on a Rigaku-Dmax 2500 diffractometer equipped with graphite monochromatized Cu Kα (λ = 0.15405 nm) radiation at a scanning speed of 4°/min in the

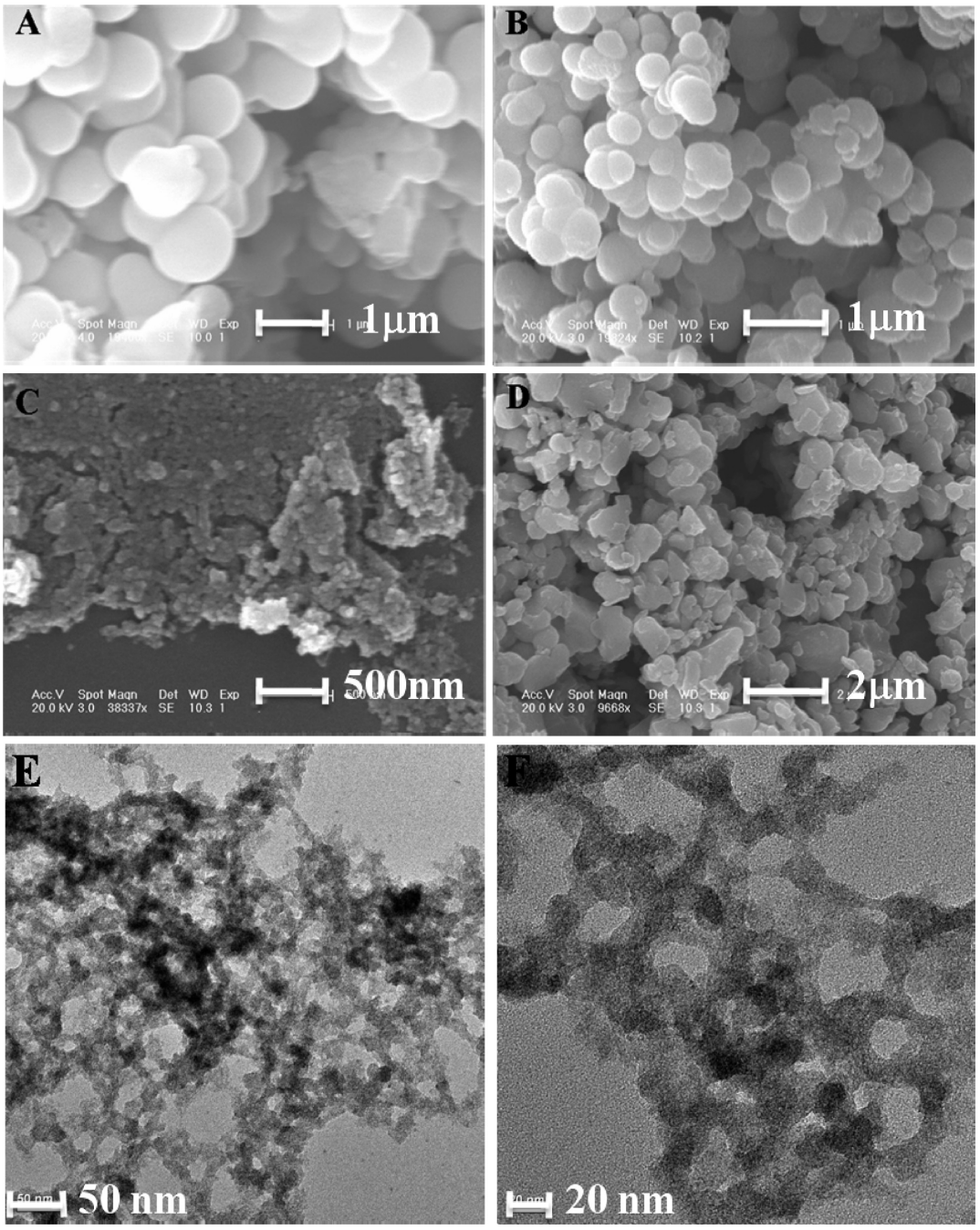

Figure 3. The typical SEM micrographs of as-prepared TiO_2 with different magnifications: (A) T-0, (B) T-01, (C) T-02, (D) T-02c. (E, F) Typical TEM micrographs of T-02.

range from 10° to 80°. Transmission electron microscopy (TEM) was carried out with Hitachi model H-8100 operating at 200 kV accelerating voltage. Scanning electron microscopy (SEM) images and energy-dispersive X-ray spectrum (EDX) were taken using Philips XL 30 and a JEOL JSM-6700F microscope. The X-ray photoelectron spectrum (XPS) was measured by using an ESCA-LAB-MKII spectrometer (UK) with Al Kα radiation (1486.6 eV) as the X-ray source for excitation.

2.4. Fabrication of Electrodes. The microporous carbon electrode material used in this paper was Maxsorb, with the B.E.T. specific surface area of 1333 $m^2\ g^{-1}$. The electrodes were fabricated by pressing the mixture of active material (TiO_2 or Maxsorb) and TAB (teflonized acetylene black) on each stainless steel mesh (1 cm^2 area).

2.5. Electrochemical measurements. Cyclic voltammetric studies were carried out on three-electrode beaker cells by CHI660C potentiostat/galvanostat. A three-electrode cell comprised a TiO_2 working electrode, a platinum flag counter electrode, and a Ag/AgCl (saturated KCl aq) reference electrode. Galvanostatic charge-discharge cycles of two-electrode coin cells (CR2032) were measured by a Land cell tester. In a two-electrode coin cell, Maxsorb and TiO_2 were taken as positive and negative electrodes, respectively. $LiClO_4$, $NaClO_4$, $KClO_4$ aqueous solutions were used as electrolytes.

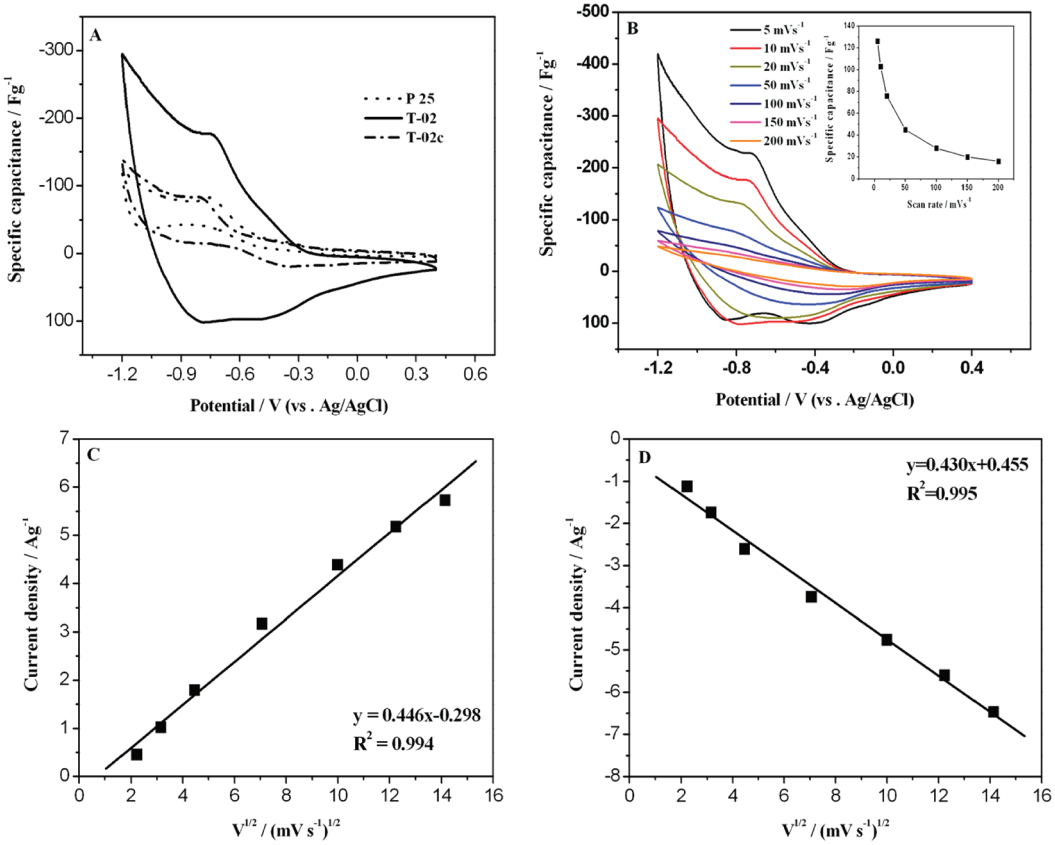

Figure 4. (A) Cyclic voltammograms of P25, T-02, and T-02c at the scan rate of 5 mV s^{-1} in the electrolyte of 1 mol L^{-1} $LiClO_4$, respectively. (B) Cyclic voltammograms of T-02 at the scan rates of 5, 10, 20, 50, 100, 150, and 200 mV s^{-1} in 1 mol L^{-1} $LiClO_4$ aqueous solution, respectively, and the relationships between the specific capacitance values and scan rates. (C) Dependency of the anodic peak currents on the square root of the potential sweep rate. (D) Dependency of the cathodic peak currents on the square root of the potential sweep rate.

3. RESULTS AND DISCUSSION

3.1. Compositions and Morphologies. The crystal structure and phase composition of the products were characterized by XRD. As shown in Figure 1A, according to the diffraction peak locations (2θ = 25.2, 37.90, 47.96, 54.32, and 63.10°) and their relative intensities, the sample T-02 could be easily indexed to anatase phase of TiO_2 (JCPDS No. 21-1272). The calculated lattice parameter for the sample is in good agreement with the known lattice parameter for crystalline TiO_2.[17] After the calcination, the intensity of the diffraction peaks is increased, indicating the improvement of crystallinity. The expanded diffraction peaks in panels A and B in Figure 1 reveal the samples of T-02 and T-02c would be nano-sized. Furthermore, the XRD patterns of other samples (T-0 and T-01) turned out to be the amorphous nature.

To further validate the elements and the corresponding valence states of titanium oxide, we characterized the samples of T-0 and T-02 by XPS. As shown in panels A and B in Figure 2, the spectrum of O1s is detected at 530.0 eV, correlating to the Ti−O−Ti bond in sample T-02. Furthermore, the doublet peaks at 458.65 and 464.4 eV are found for $Ti2p_{3/2}$ and $Ti2p_{1/2}$, indicating the Ti^{4+} state in sample T-02.[18−20] For comparison, the binding energies (BE) of O1s exhibit three peaks at 532.7, 531.45, 529.95 eV in Figure 2C, corresponding to H−O−H, Ti−OH, Ti−O−Ti at the surface of the sample T-0, respectively. In addition, the BE of Ti2p express the doublet peaks in Figure 2D at 457.85 and 463.35 eV, suggesting the existence of Ti^{3+} state in sample T-0 as well, accordance with the XRD data.[18−20] Thus, we may conclude that the participation of HPW improves the crystallinity of TiO_2.

To further prove the chemical components of the as-prepared samples, EDX chemical component measurement (T_{02}) was shown in Figure S1 (see the Supporting Information). The data confirm that the sample of T_{02} contains elements of Ti and O (note: the Au and Si related peaks in the spectrum came from the gold coating and the silicon slide, respectively, when investigating SEM), implying that the as-prepared materials are titanium oxide. In addition, the EDX analysis carried out on other samples exhibit very similar spectra revealing the chemical uniformity of the materials.

The micro-architecture of resultant TiO_2 was affected by the amount of HPW. As shown in Figure 3A, if none of any HPW (sample T-0) was introduced in our synthesis, the products are spheres in the micrometersized range, typically about 1000 nm. Increasing the concentration of HPW to 0.1 mol L^{-1} (sample T-01), the size of the spheres is decreased to submicrometersized range, typically between 100 nm and 500 nm shown in Figure 3B. Further increase the concentration of HPW to 0.2 mol L^{-1} (sample T-02), the particle size reduces to less than 20 nm in Figure 3C. The reduced size of products reveals that concentrated HPW leads to smaller-sized TiO_2 NPs. Detailed structural information of sample T-02 was detected via TEM technology.

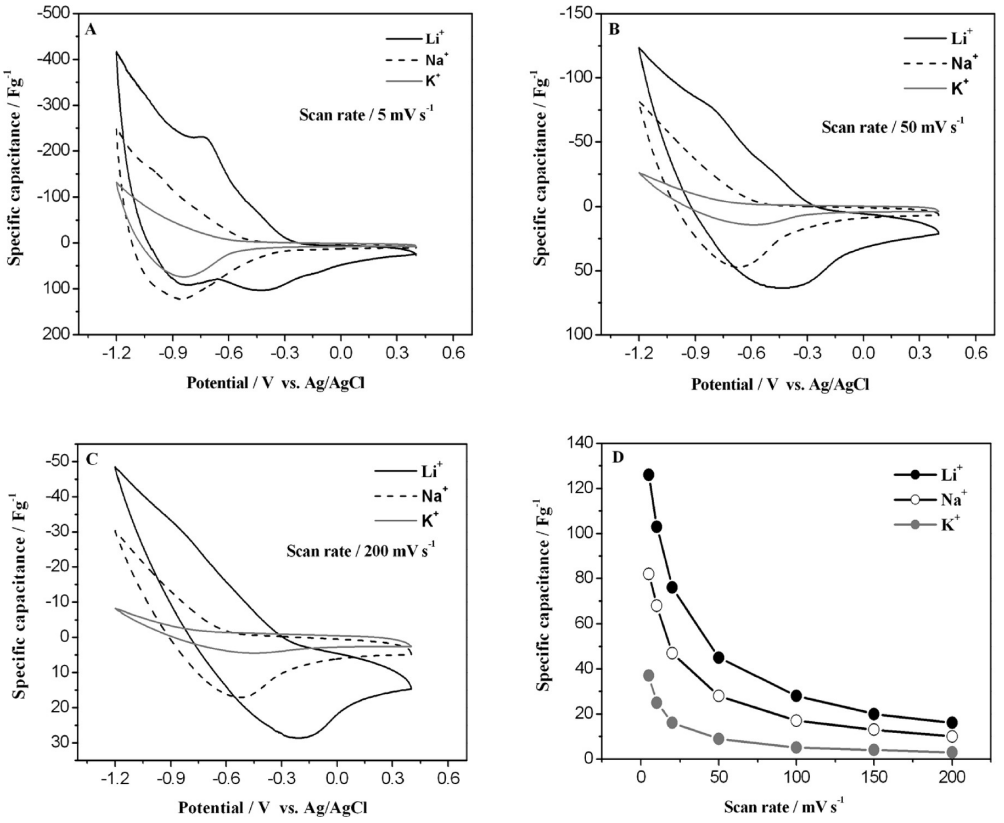

Figure 5. Cyclic voltammograms of the sample of T-02 in the electrolytes of 1 mol L^{-1} $LiClO_4$, 1 mol L^{-1} $NaClO_4$, 0.5 mol L^{-1} $KClO_4$ aqueous solutions at the scan rates of 5 mV s^{-1} (A), 50 mV s^{-1} (B), and 200 mV s^{-1} (C), respectively. Relationships between the specific capacitance values and scan rates for Li^+, Na^+, K^+ (D).

It is observed that those nano-sized particles connected each other to form network structures. After a heat-treatment, the original particles aggregated together and ripened to form bigger assembles to a certain extent. Based on the above observation, we may conclude that the quantities of HPW play an important role in determining the size of TiO_2. In addition, different concentrations of HCl, H_3PO_4, H_2SO_4, $H_2C_2O_4$, and CH_3COOH were also investigated, the size of resultant TiO_2 shows no obvious change, typically between 100 and 500 nm.

3.2. Growth Mechanism of the Products. On the basis of the data above, we proposed a HPW controlled hydrolysis mechanism to explore the formation of the nano-sized TiO_2. At the initial stage, the very rapid hydrolysis leads to a solution with a high degree of supersaturation of hydroxylated titanium (≡Ti−OH). This results in a high rate of nucleation and the formation of small particles or crystallites.[21] Aggregation will take place without the participation of acid. However, the hydroxylated titanium is protonated in strong acidic solution and the particle surface is positive charged (≡Ti−OH_2^+). The electrostatic repulsion of the charged particles prevents the aggregation of the formed small particles.[21,22] As a result, the higher acidity (0.1 mol L^{-1} HPW pH ∼4.5; 0.2 mol L^{-1} HPW pH ∼2; 0.4 mol L^{-1} HPW pH <1), the smaller particle size (the lower degree of aggregation).[23,24] Nevertheless, no precipitates were produced when the concentration of HPW reached to 0.4 mol L^{-1} because the nuclei were dissolved in such strong acidic solution.[21,22] In addition, the complexing anions ($PW_{12}O_{40}^{3-}$) of HPW can complex with protonated titanium (≡Ti−OH_2^+), which may be contributed to the slower crystallization of small particles and the further growth into anatase.[21−26] In conclusion, the strong acidity of concentrated HPW and the complexing anions of HPW are dedicated to the formation of small particles and the improved crystallization of resultant TiO_2 NPs. As for HCl, H_3PO_4, H_2SO_4, $H_2C_2O_4$ and CH_3COOH, the anions (Cl^-, PO_4^{3-}, SO_4^{2-}, $C_2O_4^{2-}$, and CH_3COO^-) may have weak complexation with protonated titanium. Thus the resultant TiO_2 emerged at a fast pace and turned out to be amorphous.

3.3. Charge Storage Mechanism and Electrochemical Performance. To evaluate the capacitive characteristics of these materials, series of electrochemical studies were performed. The cyclic voltammograms (CV) were compared in 1 mol L^{-1} $LiClO_4$ aqueous solution by means of a three-electrode cell system. As shown in Figure 4A, the similar redox peaks are observed at the negative potential window. Considering the surrounding surface area, it exhibits that the sample T-02 possesses larger specific capacitance value than that of any other samples, which might correlate with their smaller size nature. B. Dunn has proposed that the total charge storage of nanoscale TiO_2 (NPs) are made up of two proportions: the nonfaradaic contribution from the double-layer capacitance and the faradaic contributions.[13−15] Considering their low surface area (BET data), the double-layer capacitance takes up small components. The faradaic contribution originated from the ions (such as Li^+) intercalation process or the charge transfer process with surface atoms (pseudocapacitance). In most cases, the insertion process is controlled or limited by the ion diffusion rate. The second pseudocapacitive effect is mainly associated with the dimensions of

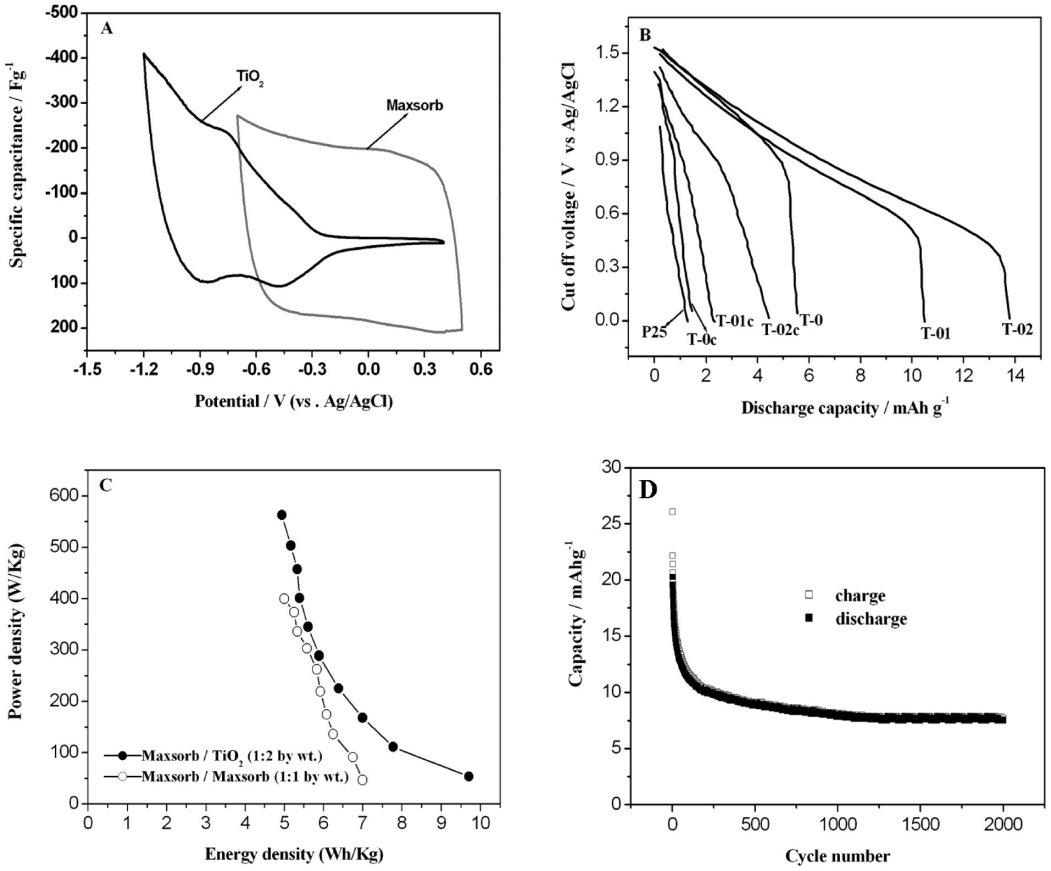

Figure 6. (A) Overlapped cyclic voltammograms of T-02 and Maxsorb in 1 mol L^{-1} $LiClO_4$ aqueous solution at the scan rate of 5 mV s^{-1}. (B) Galvanostatic discharge curves of all TiO_2 samples in 1 mol L^{-1} $LiClO_4$ aqueous solution at the constant current density of 166.67 mA g^{-1}. (C) Ragone plots of asymmetrical electrochemical capacitor composed of TiO_2 (T-02) and Maxsorb electrodes, and symmetrical electrochemical capacitor composed of two Maxsorb electrodes in the electrolyte of 1 mol L^{-1} $LiClO_4$ aqueous solution. (D) Long cycling performance of asymmetrical electrochemical capacitor composed of Maxsorb and TiO_2 (T-02) electrodes in 1 mol L^{-1} $LiClO_4$ aqueous solution at the constant current density of 166.67 mA g^{-1}.

materials. In our report, reducing the size of TiO_2 to nanoscale offers more active sites, shortens the diffusion path lengths and gives easy access to electrolyte. These advantages make good contributions to the fast charge/discharge rate. Hence we may conclude that reducing the TiO_2 dimension to nanoscale enhances the typical faradaic capacitance. Figure 4B exhibits the CVs of sample T-02 in the electrolyte of 1 mol L^{-1} $LiClO_4$ aqueous solution at the scan rates of 5, 10, 20, 50, 100, 150, and 200 mV s^{-1}, respectively. The presence of redox peaks implies the faradaic behavior. Figure 4B also depicts the relationships between the specific capacitance values and scan rates. These data imply the following trend: the lower scan rates, the bigger specific capacitance values. Panels C and D in Figure 4 display the relationship between two peak currents and the square root of the potential scan rates. Both anodic and cathodic peak currents linearly depend on the square root of the potential scan rates. This linear dependency indicates that the intercalation/deintercalation process is still controlled by lithium-ion diffusion for TiO_2 NPs, thus, the lower scan rates result in the bigger specific capacitance.

Furthermore, we also evaluated their capacitive behavior in different electrolytes at various scan rates. As shown in Figure 5A, similar anodic peaks are observed in the solutions of $NaClO_4$ and $KClO_4$ at the scan rate of 5 mV s^{-1}, indicating the partial insertion of Na^+ and K^+. However, the scan rates are further increased in Figure 5B and 5C, the anodic peaks disappear in the solutions of $NaClO_4$ and $KClO_4$. This phenomenon might be attributed to the fact that Na^+ and K^+ own bigger radius than that of Li^+. Thus, it is difficult for Na^+ and K^+ to intercalate at higher scan rates (higher current density). As a result, the specific capacitance values manifest remarkable shrinkages for Na^+ and K^+ with the increase of scan rates shown in Figure 5D. In conclusion, the comparisons further confirm the intercalation process of nano-sized TiO_2.

To validate its potential application, a hybrid capacitor consisting of a combination of TiO_2 as negative electrode, Maxsorb as positive electrode was constructed. The charge-discharge cut off voltage for AC/TiO_2 hybrid electrochemical capacitors was firstly investigated. Figure 6A shows the overlapped CVs of TiO_2 (T-02) and Maxsorb in the negative and positive portions, respectively. It illuminates that the maximal cut off voltage for asymmetrical capacitors can reach to 1.7 V (vs. Ag/AgCl). To conduct the long cycles of galvanostatic charge-discharge, the cut off voltage is set as 1.6 V in the following charge-discharge tests. As shown in Figure 6B, the T-02 (NPs) exhibits high gravimetric energy density than that of other samples (P25, T-0, T-0c, T-01, T-01c, and T-02c), accordantly with its small-sized nature. Furthermore, the shapes of the discharge curves of these capacitor

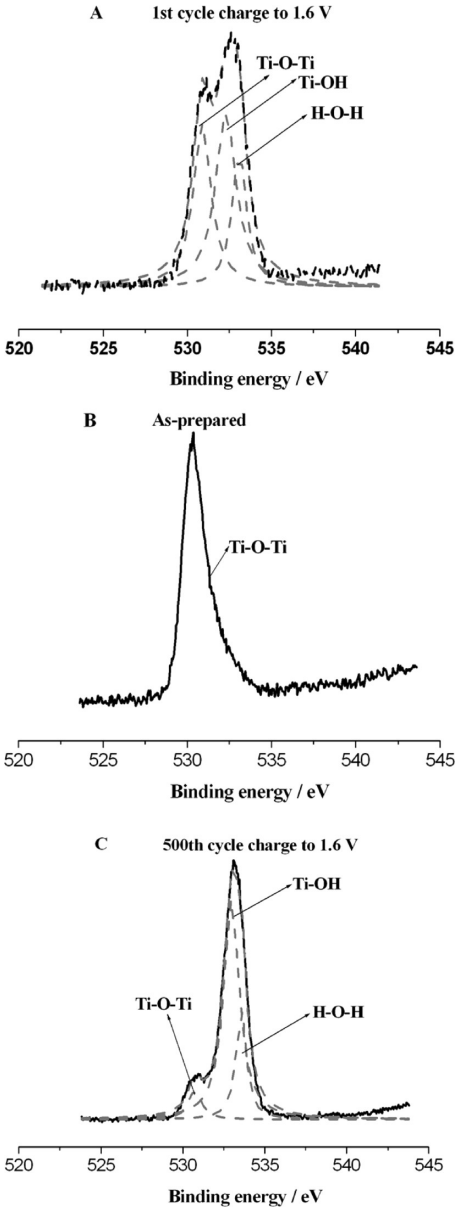

Figure 7. Ex situ XPS spectra of O1s for reduced, as-prepared composite electrodes at different charge-discharge cycles. Mixed Lorentzian fitting peaks (dotted curves).

systems are bent curves instead of straight lines and the discharge capacity is dropped sharply at lower voltage because the intercalation of lithium ions occurs at negative potential portions for TiO_2. These facts also indicate the faradaic processes of nano-sized TiO_2 in aqueous electrolyte. In addition, the discharge curve (straight line) of symmetrical capacitor (AC/AC) was also displayed in Figure S2 (see the Supporting Information), which reveals the non-faradaic capacitive behavior (physical adsorption) of activated carbon. Next, to compare the energy density and power density of hybrid AC/TiO_2 (T-02) and symmetrical AC/AC capacitors, the Ragone plots of two capacitors are displayed in Figure 6C. To obtain authentic data, we performed the Ragone plot of the hybrid AC/TiO_2 (T-02) capacitor after 20 continuous cycles at the constant current density of 166.67 mA g^{-1}. The energy density and power density were evaluated from the galvanostatic discharge curves by taking account the total mass of both electrode active materials. The hybrid AC/TiO_2 capacitor has both higher energy density and power density (9.7 Wh kg^{-1}, 563 W kg^{-1}) than that of symmetrical AC/AC capacitor (7.0 Wh kg^{-1}, 399.9 W kg^{-1}). Furthermore, the long cycling tests of hybrid AC/TiO_2 (T-02) and symmetrical AC/AC capacitors are shown in Figure 6D and Figure S3 (see the Supporting Information), respectively, it reveals that the hybrid capacitor also has stable cycling life after 2000 continuous charge-discharge tests.

However, the capacity is dropped sharply before 200 cycles and tends to be stable after 500 cycles with relative low capacity retention. To explore the reasons for this capacity shrinkage, Ex-situ XPS Surface Analysis of the composite electrodes was performed. The previous studies had demonstrated that the O1s had greater validation for surface analysis of electrodes.[27,28] Hence, the O1s core level spectrum can be used to assess the state change of TiO_2 during the oxidized and reduced processes. The data are fully listed in Table S2 (see the Supporting Information). As comparison, the TiO_2 electrode was charged to 1.6 V, the bonding energy of O1s shifts to the higher energy area, which is deduced to the bonds of Ti−O−Ti (530 eV, 34.3%), Ti−OH (531.5 ± 0.5 eV, 42.9%), H−O−H (533 ± 1 eV, 22.8%),[20,29] respectively.

After a continuous extension of charge−discharge process (500 cycles), the percentages of Ti−OH bond increase sharply to 70.0% with the decrease of Ti−O−Ti (7.6%) bond. These phenomena confirm the fact that the irreversible intercalation of lithium ions reduces the Ti^{4+} to Ti^{3+} largely and increases the content of hydroxyl groups at the surface. In a word, the ex situ XPS surface analysis of the composite electrodes reveals the irreversible lithium intercalation reaction in aqueous solution which results in the capacity reduction.

4. CONCLUSION

In summary, polyoxometalate (HPW) assisted hydrolysis of TBT for synthesizing TiO_2 NPs has been described. Concentrated HPW resulted in TiO_2 NPs. The electrochemical tests demonstrated that TiO_2 NPs possessed higher energy density than that of other TiO_2 samples. In addition, the intercalation mechanism of resultant TiO_2 NPs in neutral salt aqueous electrolytes was testified via cyclic voltammetry, galvanostatic cycling tests. The TiO_2 NPs were conducted to assemble hybrid capacitor with activated carbon. The hybrid capacitor constructed from AC/TiO_2 showed an average cell potential of 1.7 V in aqueous solution. Furthermore, the hybrid AC/TiO_2 (NPs) capacitor possessed both higher energy density and power density (9.7 Wh kg^{-1}, 563.0 W kg^{-1}) than that of symmetrical AC/AC capacitor (7.0 Wh kg^{-1}, 399.9 W kg^{-1}). The hybrid AC/TiO_2 electrochemical capacitor had stable cycling life after 2000 cycles. Finally, ex situ XPS surface analysis of the TiO_2 electrodes was performed to explore the capacity shrinkage during the long cycling tests. It reveals the irreversible lithium intercalation reaction in aqueous solution, which results in the capacity reduction.

■ ASSOCIATED CONTENT

Supporting Information. Sample names of prepared TiO_2 under different conditions, EDX spectrum of T-02, galvanostatic discharge curve of Masorb in 1 mol L^{-1} $LiClO_4$ aqueous solution at the constant current density of 166.67 mA g^{-1}, long cycling performance of symmetrical AC/AC capacitor in 1 mol

L^{-1} $LiClO_4$ aqueous solution at the constant current density of 166.67 mA g^{-1}, data obtained from the XPS Spectrum shown in Figure 7. This material is available free of charge via the Internet at http://pubs.acs.org/.

AUTHOR INFORMATION

Corresponding Author
*Tel/Fax: 86-431-85262287. E-mail: hongyuwang@ciac.jl.cn.

ACKNOWLEDGMENT

This project was supported by the Foundation of Applied science and technology of Jilin Province (20090521), National Basic Research Program of China (2011CB935702) and Hundred Talents Program of Chinese Academy of Sciences.

REFERENCES

(1) Simon, P.; Gogotsi, Y. *Nat. Mater.* **2008**, *7*, 845–854.
(2) Zhang, Y.; Feng, H.; Wu, X. B.; Wang, L. Z.; Zhang, A. Q.; Xia, T. C. *Int. J. Hydrogen Energy* **2009**, *34*, 4889–4899.
(3) Kotz, R.; Carlen, M. *Electrochim. Acta* **2000**, *45*, 2483–2498.
(4) Zheng, J. P.; Jow, T. R. *J. Power Sources* **1996**, *62*, 155–159.
(5) Pell, W. G.; Conway, B. E. *J. Power Sources* **2004**, *136*, 334–345.
(6) Sikha, G.; Popov, B. N. *J. Power Sources* **2004**, *134*, 130–138.
(7) Wang, H.; Yoshio, M.; Thapa, A.; K. Nakamura, H. *J. Power Sources* **2007**, *169*, 375–380.
(8) Zhao, X.; Sanchez, B. M.; Dobson, P. J.; Grant, P. S. *Nanoscale* **2011**, *3*, 839–855.
(9) Trigueiro, J. P. C.; Borges, R. S.; Lavall, R. L.; Calado, H. D. R.; Silva, G. G. *Nano Res.* **2009**, *2*, 733–739.
(10) (a) Chen, J. S.; Tan, Y. L.; Li, C. M.; Lou, X. W. *J. Am. Chem. Soc.* **2010**, *132*, 6124–6130. (b) Lou, X. W.; Archer, L. A. *Adv. Mater.* **2008**, *20*, 1853. (c) Lunell, S.; Stashans, A.; Ojamae, L.; Lindstrom, H.; Hagfeldt, A. *J. Am.Chem. Soc.* **1997**, *119*, 7374. (d) Chen, J. S.; Lou, X. W. *Electrochem. Commun.* **2009**, *11*, 2332. (e) Yang, Z. G.; Choi, D. W.; Kerisit, S.; Rosso, K. M.; Wang, D. H. *J. Power Sources* **2009**, *192*, 588–598.
(11) (a) Chen, J. S.; Lou, X. W. *J. Power Sources* **2010**, *195*, 2905. (b) Dambournet, D.; Belharouak, I.; Amine, K. *Chem. Mater.* **2010**, *22*, 1173–1179.
(12) Arico, A. S.; Bruce, P.; Scrosati, B.; Tarascon, J. M.; Schalkwijk, M. V. *Nat. Mater.* **2005**, *4*, 366.
(13) Kang, J.; Wei, S. H.; Zhu, K.; Kim, Y. H. *J. Phys. Chem. C* **2010**, *115*, 4909–4915.
(14) Brezesinski, T.; Wang, J.; Polleux, J.; Dunn, B. *J. Am. Chem. Soc.* **2009**, *131*, 1802–1809.
(15) Lindstrom, H.; Sodergren, S.; Solbrand, A.; Rensmo, H.; Hjelm, J.; Hagfeldt, A.; Lindquist, S. E. *J. Phys. Chem. B* **1997**, *101*, 7717.
(16) Reiman, H. K.; Brace, K. M. *Electrochem. Commun.* **2006**, *8*, 517–522.
(17) Dai, Y. Q.; Cobley, C. M.; Zeng, J.; Sun, Y. M.; Xia, Y. N. *Nano Lett.* **2009**, *9*, 2455–2459.
(18) Moulder, J. F.; Stickle, W. F.; Sobol, P. E. *Handbook of X-ray Photoelectron Spectroscopy*, 2nd ed.; Perkin-Elmer Corporation: Eden Prairie, MN, 2002.
(19) Gouttebaron, R.; Cornelissen, D.; Snyders, R.; Dauchot, J. P.; Wautelet, M.; Hecq, M. *Surf. Interface Anal.* **2000**, *30*, 527–530.
(20) Sanjines, R.; Tang, H.; Berger, H.; Gozzo, F.; Margaritondo, G.; Levy, F. *J. Appl. Phys.* **1994**, *75*, 2945–2951.
(21) (a) Bischoff, B. L.; Anderson, M. A. *Chem. Mater.* **1995**, *7*, 1772–1778. (b) Suttiponparnit, K.; Jiang, J. K.; Sahu, M.; Suvachittanont, S.; Charinpanitkul, T.; Biswas, P. *Nanoscale Res. Lett.* **2011**, *6*, 27.
(22) Sugimoto, T.; Zhou, X. P.; Muramatsu, A. *J. Colloid Interface Sci.* **2002**, *252*, 339–346.
(23) Isley, S. L.; Penn, R. L. *J. Phys. Chem. C* **2008**, *112*, 4469–4474.
(24) Pottier, A.; Cassaignon, S.; Chaneac, C.; Villain, F.; Jolivet, J. P. *J. Mater. Chem.* **2003**, *13*, 877–882.
(25) Huang, D.; Wang, Y. J.; Yang, L. M.; Luo, G. S. *Microporous Mesoporous Mater.* **2006**, *96*, 301–306.
(26) Pozniczek, J.; Micek-Ilnicka, A.; Lubanska, A. *Appl. Catal., A* **2005**, *286*, 52–60.
(27) Chigane, M.; Ishikawa, M. *J. Electrochem. Soc.* **2000**, *147*, 2246.
(28) Chigane, M.; Ishikawa, M.; Izaki, M. *J. Electrochem. Soc.* **2001**, *148*, D96–D101.
(29) Sodergren, S.; Siegbahn, H. *J. Phys. Chem. B* **1997**, *101*, 3087–3090.